Radiowave and microwave frequency dielectric relaxations at the superionic, incommensurate and ferroelectric phase transitions in NH_4HSeO_4 and ND_4DSeO_4

1992 J. Phys.: Condens. Matter 4 5625

(http://iopscience.iop.org/0953-8984/4/25/016)

J. Phys.: Condens. Matter 4 (1992) 5625–5638. Printed in the UK

Radiowave and microwave frequency dielectric relaxations at the superionic, incommensurate and ferroelectric phase transitions in NH_4HSeO_4 and ND_4DSeO_4

Ph Colomban†§ and J C Badot‡

† Laboratoire de Physique de la Matière Condensée (URA 1254, CNRS), Ecole Polytechnique, 91128 Palaiseau, France

‡ Laboratoire de Chimie Appliquée de l'Etat Solide (URA 1466, CNRS), ENSCP, 11 rue Pierre et Marie Curie, 75231 Paris Cédex 05, France

Received 4 September 1991, in final form 16 December 1991

Abstract. Ammonium hydrogen selenates NH_4HSeO_4 (AHSe) and ND_4DSeO_4 (ADSe) have been studied in the radiowave and microwave frequency ranges by network and impedance analysers between 200 and 410 K. Three relaxations of about 5×10^{-8}, 5×10^{-10} and 5×10^{-11} s have been observed and assigned to reorientations of ammonium ions, proton jumps and reorientations of selenate ions, respectively. The corresponding dielectric susceptibilities have been studied and mechanisms for the different phase transitions from the superionic phase to the paraelectric, incommensurate and ferroelectric phases have been proposed. The origin of metastable phases and of memory effect is discussed.

1. Introduction

Ammonium hydrogen selenate NH_4HSeO_4 (AHSe) appears interesting since it undergoes phase transitions from the high-temperature superionic ($T > 409$ K) to the paraelectric, incommensurate and ferroelectric phases. This compound and its deuterated derivative ND_4DSeO_4 (ADSe) have been extensively studied, particularly by the groups at Krasnoyarsk (Aleksandrov *et al* 1980, Aleksandrova *et al* 1983, 1986) and Wrocław (Czapla *et al* 1979, 1984). In recent work we have proposed a new phase diagram (Colomban *et al* 1988), essentially similar for both AHSe and ADSe, and confirmed by x-ray and neutron diffraction, nuclear magnetic resonance, infrared and Raman spectroscopies (Aleksandrova *et al* 1989).

The aim of our work is to understand the phase transition mechanisms with special emphasis on the dynamics of protonic species. However, structural knowledge of the host lattice and of the protonic species is not sufficient for the understanding of charge transfer in solids and we have undertaken a comprehensive study of the proton dynamics in typical, more or less crystalline, protonic conductors (Colomban and Novak 1988, Colomban and Badot 1992). By performing electrical measurements continuously over the radiowave and microwave frequency range (1 MHz–10 GHz), it is possible to ascertain direct information about charge motions along pathways

§ Present address: ONERA-OM, BP72, 92322 Chatillon Cédex, France.

0953-8984/92/255625+14$04.50

from the order of the bond length to several bond lengths. Preliminary results on NH_4HSeO_4 have shown that protons, NH_4^+ and $HSeO_4^-$ ions have opposite types of behaviour with respect to incommensurate phase transitions (Badot and Colomban 1989). In this paper we report a detailed comparison of AHSe and ADSe and we attempt to explain phase transition mechanisms in structures with mobile charges.

2. Experimental details

NH_4HSeO_4 (AHSe) and ND_4DSeO_4 (ADSe) crystals were grown by cooling saturated aqueous solutions (Colomban *et al* 1988). All crystals were colourless and, being slightly hygroscopic, were kept in sealed bottles. Crystals were ground in an agate mortar under a dry atmosphere and compacted by room-temperature pressure sintering (300 MPa, 1 hour) into dense translucent pellets (diameter 3 mm, thickness 0.5 mm). A layer of Pt paint a few microns thick was deposited on each face at room temperature. Pellets were then annealed for at least a week at room temperature in a sealed bottle in order to eliminate possible modifications induced by pressure.

The electrical cell is a circular coaxial line whose inner conductor is interrupted by a pellet of the same diameter and loaded by a short circuit. The electric field is parallel to the common axis of the sample pellet and of the inner conductor, as fully described by Badot *et al* (1985). The dielectric studies have been performed in a broad frequency range from 1 MHz to 10 GHz using different automatic devices: an RF impedance analyser model HP4191A and network analyser models HP8410 and/or 8510.

A home-made cryostat and hot cell allow us to explore the 180–450 K temperature range; a confined N_2 dry atmosphere is used. In this temperature range the electromagnetic properties of coaxial lines and dilatometric variation do not decrease the accuracy of the measurements significantly. Our investigations have been limited to 405 K to prevent the D/H exchange owing to the increase of the proton mobility occurring in the superionic phase.

3. Results and discussion

3.1. Phase diagrams and structures of AHSe and ADSe

The relationship between stable (VI, II, I) and metastable (V′, IV′, III′ and II′ on cooling) phases together with the transition temperature is shown in figure 1. The metastable phases are gradually transformed into stable ones by annealing at appropriate temperatures (Colomban *et al* 1988). The temperatures of the phase transitions of AHSe and ADSe generally vary by a few degrees, the largest difference being observed for the VI⟶II transition, 350 and 330 K for ADSe and AHSe, respectively. This may imply that OH...O proton ordering does not correspond to the main mechanism creating the ferroelectric phase IV′ and that the ordering of ammonium ions as well as of selenate ions should be considered.

The paraelectric phase II is monoclinic and belongs to the B_2 (C_2^3) space group. The structure consists of infinite chains of $HSeO_4^-$ anions linked by strong OH...O hydrogen bonds. The results of x-ray diffraction (Aleksandrov *et al* 1980) and of vibrational spectroscopy (Aleksandrova *et al* 1989, Pasquier *et al* 1990) show that there are three types of structural disorder: (i) translational disorder of the proton

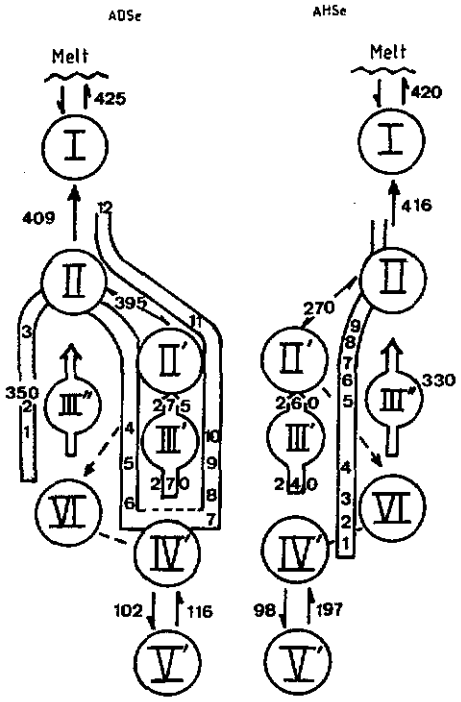

Figure 1. Diagrammatic representation of phase transitions in AHSe and ADSe. Metastable phases are designated with a prime: I, superionic phase; II, paraelectric phase (B2); III′ and III″, incommensurate or modulated phases; IV′, ferroelectric phase (B1); VI, orthorhombic phase ($P2_12_12_1$); the Arabic number corresponds to the successive measurements.

in OH...O hydrogen bonds and orientational disorder of (ii) ammonium and (iii) selenate ions. The ferroelectric phase IV′ results from a small distortion of the monoclinic B2 structure, the spontaneous polarization being parallel to the *b*-axis ($HSeO_4^-$ chain direction). The crystalline structure of the phase V′ has not been determined. From vibrational spectroscopy it can be concluded that the $HSeO_4^-$ motions appear important at both ends of the sequence; that is in the V′ ⟶IV′ and II⟶I transitions. The VI⟶II transition seems to correspond to gliding motions of ammonium ions along the *b*-chain axis followed by a reorientation of $HSeO_4^-$ ions (Aleksandrova *et al* 1989).

Appropriate temperature cycles must be performed to observe clearly the phase transition by minimizing the traces of the phase of the sequence that is not considered. It should be pointed out that at room temperature AHSe is in phase II′ whereas ADSe is in phase VI. The cycles are indicated in figure 1, the numbers in braces corresponding to the successive measurements:

(i) AHSe: the pellet is heated at 350 K (to phase II) and then cooled and kept for a week at 250 K. The pellet is rapidly cooled to 190 K {1} and measurements are then made on heating at 203 {2}, 238 {3}, 250 {4}, 260 {5}, 270 {6}, 297 {7}, 320 {8} and 350 K {9} in order to study the IV′ ⟶III′ ⟶II′ sequence.

(ii) ADSe: the sample annealed at 300 K for a week is measured successively at 293 {1}, 353 {2}, 383 {3}, 300 {4}, 270 {5} and 240 K {6}. After that the pellet is

kept for a week at 230 K and measurements are made on heating: 200 {7}, 258 {8}, 280 {9}, 300 {10}, 380 {11} and 408 K {12}.

3.2. Evidence of various dielectric relaxations

The measurements are shown in figure 2. The $\epsilon'' = f(\epsilon')$ representation is used to have a clear-cut distinction between features arising from fixed charges (i.e. high-frequency relaxations) and those from the long-range mobile charges (low-frequency to DC conduction). In some cases the $\epsilon'' = f(\epsilon')$ recorded spectra give evidence for a well shaped semicircle and for a low-frequency straight line. This has been observed for many proton conductors in which the various dipoles are of the same order of magnitude (Badot *et al* 1987, 1991, Badot and Colomban 1989). In our case, except for the 270 K {5} and 258 K {8} data, the substitution of the conduction loss is required to obtain a visible separation between the 'free charge' and the dipolar contributions (figure 3). We have extensively discussed the deconvolution procedure in a previous paper (Badot *et al* 1985). The substitution of the conduction losses makes the assumption that all the dipolar contributions are additive and that the $\epsilon'' = f(\epsilon')$ plot may be formed, for a good ionic conductor, by a straight line at low frequency, representing the conductivity σ_{DC} and that additional contributions at high frequency are the result of various relaxations (Dygas and Brodwin 1985, Richards 1977, Volkov *et al* 1989). According to the classical Debye model the straight line intercepts the ϵ'-axis at ϵ_s, the static permittivity.

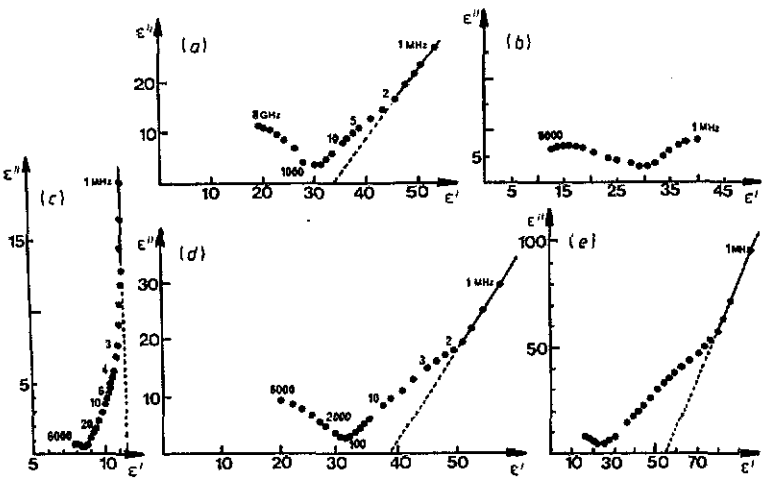

Figure 2. Experimental Cole–Cole plots for ADSe in different phases: (*a*), 353 K; (*b*), 270 K; (*c*), 293 K; (*d*), 383 K; (*e*), 408 K.

Figure 3 shows typical Cole–Cole plots $\epsilon'' = f(\epsilon')$ for ADSe in different phases. Cole–Cole plots for AHSe have been made previously (Badot and Colomban 1989). Four types of phenomena are observed. Domain 1 corresponds to the conduction loss divergence, and the conductivity can be deduced from the relation $\sigma = \omega\epsilon_0\epsilon''$. This domain can be observed in the MHz range only if the conductivity is sufficiently high. When this is not the case, the straight line in the figure has been assumed by extrapolation and serves as a visual guide. In many cases the angle of the straight line with the abscissa differs slightly from $\pi/2$ and controversial interpretations are

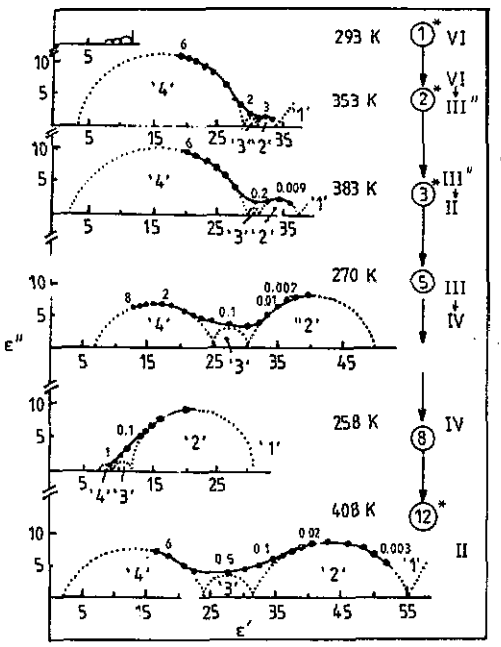

Figure 3. Calculated Cole–Cole plots, $\epsilon'' = f(\epsilon')$, for ADSe in different phases; • indicates that the domain '1', corresponding to the conduction loss divergence, has been subtracted for convenience. The 270 and 258 K spectra are the experimental data. Frequencies are given in GHz.

possible as discussed in Jonsher (1983). The low-frequency conductivity can be used to control the nature of the phase, by comparison with previous works (Badot and Colomban 1989). The low-frequency conductivity can be calculated from the data below 1 MHz. At 300 K the conductivity of ADSe is equal to 10^{-3} S m^{-1} with an activation energy (0.1 eV) constant up to 380 K; that is in the sequence VI⟶II. In the other sequences the conductivity is too low ($\leqslant 10^{-5}$ S m^{-1}) to be measured with our equipment. At 380 K {11} the conductivity is slightly lower than for point {3} and the activation energy up to 408 K is equal to 0.16 eV. At 300 K the conductivity of NH_4HSeO_4 is about 10^{-2} S m^{-1} with an activation energy of 0.4 eV. A lower activation energy (0.1 eV) is observed below 260 K (the sequence IV′ ⟶II). In phase II the conductivity decreases, the conductivity being slightly higher for AHSe than for ADSe. The conductivity of ND_4DSeO_4 in the VI⟶II sequence (i.e. the superionic transition) is 10^3 times higher than those observed for $CsHSO_4$ and for $CsDSO_4$ (Badot and Colomban 1989), according to previous measurements at fixed frequencies (Baranov *et al* 1982, Moskvich *et al* 1984, Hainovsky and Hairetdinov 1985).

Semicircles and/or circular arcs (the centre of the circle is off centre of the abscissa) are characteristic of Debye and non-Debye relaxations, respectively, and can be described using the Debye formalism†:

$$\epsilon^*(\omega) = \epsilon_\infty + \{(\epsilon_1 - \epsilon_\infty)/[1 + (i\omega\tau_1)^{\beta_1}]\} + \{[\epsilon_2 - \epsilon_1] /[1 + (i\omega\tau_2)^{\beta_2}]\} + \ldots + \{[\epsilon_s - \epsilon_n]/[1 + (i\omega\tau_n)^{\beta_n}]\} + A(i\omega)^{s-1}$$

† The conduction loss contribution $A(i\omega)^{s-1}$ ($s \simeq 0.5$–0.8) only occurs in (ionic) conductors (Jonsher 1983).

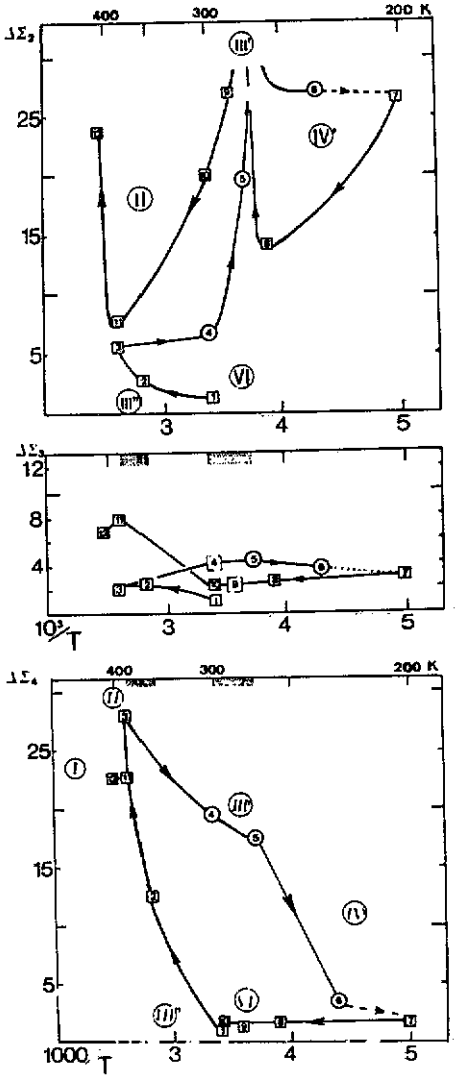

Figure 4. Dielectric susceptibility plots against inverse temperature ($\Delta\epsilon_n = f(10^3/T)$ for each type of relaxation in ADSe: $\Delta\epsilon_2$ (ND_4^+ relaxation), $\Delta\epsilon_3$ (proton jump relaxation) and $\Delta\epsilon_4$ ($DSeO_4^-$ relaxation). The dotted regions at the top show the temperature range of phases III′ and III″, which are detected by calorimetry measurements (Colomban *et al* 1988).

where ϵ_∞ and ϵ_s are limiting values when ω approaches the optical and static values, respectively. $\epsilon_1, \epsilon_2, \ldots, \epsilon_n$ are the successive intersections with the real ϵ'-axis. τ_n is known as the (Debye) relaxation time deduced from the loss-peak frequency $f_{pn} = (2\pi\tau_n)^{-1}$. β_n is an empirical parameter, which measures the degree of departure from the Debye model ($0 \leqslant \beta \leqslant 1$). $\Delta\epsilon = \epsilon_n - \epsilon_{n-1}$ ($= \epsilon_s - \epsilon_\infty$, if only one relaxation occurs) represents the orientational electric susceptibility of each relaxation. The ϵ_∞-value is determined by extrapolation of the circular arc observed on the high-frequency side. Our ϵ_∞ is thus an approximation on the high-frequency side, additional features being possible in the 10–100 GHz range (new relaxation,

Cole–Davidson behaviour, resonance,...).

In both AHSe and ADSe, three relaxations are observed. The $\Delta\epsilon$ change as a function of the temperature is particularly evident, especially for relaxations numbers 2 and 4.

3.3. Assignment of the relaxations

The first problem to solve is the assignment of each relaxation. The first step is to identify the species that can induce relaxations at these frequencies; that is polar entities and/or mobile charges. The most efficient criterion is to compare materials with similar structures and conductivities but containing various entities. For example, in previous studies a comparison of $H_3OUO_2PO_43H_2O$ and $NaUO_2PO_43H_2O$ Cole–Cole plots has allowed us to determine the reorientation of H_3O^+ and H_2O molecules (Badot *et al* 1987). Comparison of $CsHSeO_4$, $CsDSeO_4$ and $CsHSO_4$ (Badot and Colomban 1989) allows us to ascribe the semicircle at 5–10 GHz to (D)HXO_4^- relaxation and the arc of the circle at 50–150 MHz to proton-jump-associated relaxation. Relaxation times for each type of entity are roughly independent of the structure and correlations have been made (Colomban and Novak 1988, Colomban and Badot 1992) for relaxation times and their activation energies as a function of the temperature.

In this way, as discussed in a preliminary report (Badot and Colomban 1989), we propose to assign relaxation domains 4 and 3 to H(D)SeO_4 reorientation and H/D jump-associated relaxation, respectively. $HSeO_4$ tetrahedra are hydrogen bonded forming infinite chains. Inversion of the hydrogen bond, that is the proton jump, leads to the formation of an instant dipole (proton jump relaxation) before the environment accommodates the new configuration by reorientation of other species. The slow relaxation of domain 2 (MHz range) is not observed in CsH(D)S(Se)O_4 and can be assigned to $NH_4(ND_4)$ relaxation. Regular (Td) NH_4^+ or ND_4^+ ions do not have permanent dipoles but structural distortion can induce them. This kind of relaxation can correspond to a reorientation (or a local) jump. Type-2 and type-3 relaxations are constituted by well centred semicircles on the abscissa, which indicates a 'clear' Debye relaxation. On the other hand, H(D)SeO_4^- reorientations have their centres below the abscissa. The β-values are typically between 0.8 and 0.85 (see table 1).

3.4. Phase transitions and dielectric susceptibility change

Figure 4 shows the dielectric susceptibility plots against inverse temperature ($\Delta\epsilon_n = f(10^3/T)$) for each type of relaxation in ADSe. Typical dielectric susceptibility plots for AHSe have been given by Badot and Colomban (1989). Temperatures are assumed to be along the pathway explained in figure 1. The dielectric susceptibility is directly related to the square of the dipole moment ($\Delta\epsilon \propto N\mu^2$) (Debye 1945, Lines and Glass 1979). Dielectric susceptibility changes are thus directly related to the change of the dipole orientation, the distortion of the entities and the jump distance in the case of relaxation associated with charge jumps.

In both AHSe and ADSe the important changes of the dielectric susceptibility are observed at the II⟵III′ ⟶IV′ and VI⟵III″ ⟶II transitions for ammonium relaxation. A divergence seems to occur in phase III′, which is consistent with a ferroelectric to paraelectric transition. On the other hand, the $DSeO_4^-$ relaxation is mainly affected at the VI⟵III″ ⟶II transitions. These can result from the displacement of both NH_4^+ and $HSeO_4^-$ ions observed by vibrational spectroscopy

Table 1. Relaxation times, activation energies and dielectric susceptibilities in ADSe.

Domains	T (K)	β	$\tau(s)$	$\tau'(s)$	E_a (eV)	$\Delta\epsilon$
2	293{1}	1	3.16×10^{-8}			1.3
	353{2}	1	1.74×10^{-8}			2.5
	383{3}	0.8	1.58×10^{-8}			5.5
	300{4}	1	3.98×10^{-8}			6.7
	270{5}	1	1×10^{-7}			20
	240{6}	1	1.38×10^{-7}			27
	200{7}	1	1.52×10^{-7}			26
	258{8}	1	1×10^{-7}			18.7
	280{9}	1	1.20×10^{-7}			27
	300{10}	1	5.50×10^{-8}			20
	380{11}	0.8	3.47×10^{-8}			7.9
	408{12}	0.8	1×10^{-7}			23.8
3	293{1}	0.8	2.88×10^{-9}	2.29×10^{-9}	0.4	1
	353{2}	1	5.67×10^{-10}	1.25×10^{-10}	0	2.4
	383{3}	1	3.98×10^{-10}	1.25×10^{-10}	0	2
	300{4}	1	6.30×10^{-10}	1.44×10^{-10}	0.2	3.6
	270{5}	1	1.45×10^{-10}	2.88×10^{-10}	0.2	4.4
	240{6}	1	3.9×10^{-9}	1×10^{-9}	0.2	3.6
	200{7}	0.8	7.94×10^{-9}	3.80×10^{-9}	0.2	3
	258{8}	0.8	1×10^{-8}			2.8
	280{9}	0.8	4.79×10^{-9}			2.5
	300{10}	1	1.51×10^{-9}			2.5
	380{11}	1	3.98×10^{-10}	1×10^{-10}	0	8
	408{12}	1	3.8×10^{-10}	1×10^{-10}	0	7
4	293{1}	0.8	7.94×10^{-11}			0.8
	353{2}	0.8	1.74×10^{-11}			13.5
	383{3}	0.8	1.45×10^{-10}			29
	300{4}	0.8	3.00×10^{-11}			20
	270{5}	0.9	4.17×10^{-11}			18.5
	240{6}	0.8	2.51×10^{-11}			3.8
	200{7}	0.8	2.29×10^{-11}			1.9
	258{8}	0.8	5.00×10^{-11}			1.8
	280{9}	0.8	5.75×10^{-11}			1.5
	300{10}	0.8	5.75×10^{-11}			2
	380{11}	0.8	2.00×10^{-11}			24
	408{12}	0.8	2.00×10^{-11}			24

(Aleksandrova *et al* 1989). The variation of $\Delta\epsilon_3$ is not large, which confirms that proton ordering is not the leading mechanism for the IV⟶II phase transitions. However, all the transitions induce a change in $\Delta\epsilon_3$, according to the evolution of the hydrogen bond shown by infrared spectroscopy (Aleksandrova *et al* 1989, Pasquier *et al* 1990).

A large variation of $\Delta\epsilon_4$ is observed at the VI⟶II phase transition and it can be expected as observed for $CsHSO_4$ that the increase in $\Delta\epsilon_4$ continues at the II⟶I transition. This is consistent with the strong modification occurring at the superionic transition: $(H(D)SeO_4)_n^-$ chains are broken and a rapid reorientation of $H(D)SeO_4^-$ ions supports the fast proton conduction and denotes plastic behaviour. The $H(D)SeO_4^-$ susceptibility is constant between 200 and 300 K on heating. It seems that the susceptibility decreases slowly on cooling along the II⟶IV′ sequence.

3.4.1. Memory effects. The dielectric stiffness associated with NH_4^+ (ND_4^+) relaxation ($1/\Delta\epsilon_2$) and with proton (deuteron) relaxation ($1/\Delta\epsilon_3$) is plotted against temperature in figure 5 for AHSe and ADSe, respectively. For AHSe the dielectric stiffness of the domain 3 relaxation (H^+ jump) shows a first-order para/ferroelectric phase transition with a transition temperature $T_c = 250$ K, an extrapolated Curie–Weiss temperature $T_0 = 240$ K and a Curie constant of $C_3 = 90$ K. However, the same transition for NH_4^+ (domain 2) is more efficient: the extrapolated Curie temperature is $T_0 = 160$ K and the Curie constant is $C = 500$ K. The large discrepancy between T_0 and T_c denotes the existence of a metastable non-polar phase below T_c.

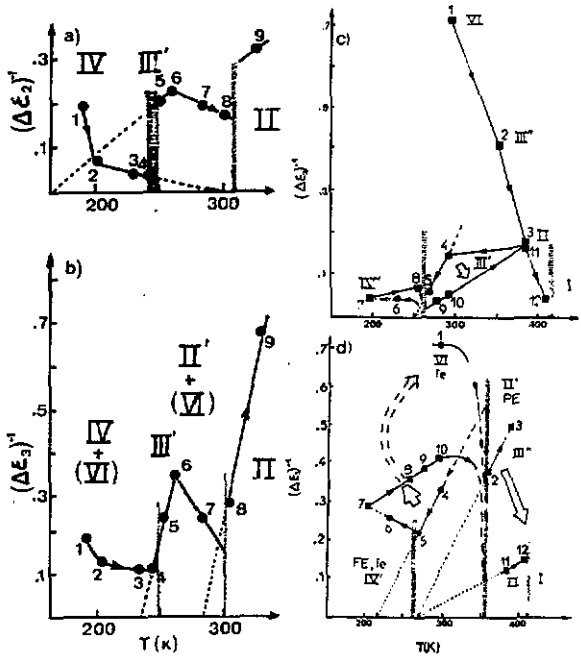

Figure 5. Plots of dielectric stiffness in AHSe ((*a*) and (*b*)) and ADSe ((*c*) and (*d*)) against temperature associated with: (*a*), NH_4^+ type-2 relaxation ($1/\Delta\epsilon_2$); (*b*), proton type-3 relaxation ($1/\Delta\epsilon_3$); (*c*), ND_4^+ type-2 relaxation ($1/\Delta\epsilon_2$); (*d*) D^+ type-3 relaxation ($1/\Delta\epsilon_3$). (FE, 'macroscopic' ferroelectric behaviour; fe, 'microscopic' ferroelectric behaviour, PE, paraelectric phase).

The dielectric stiffness $(\Delta\epsilon_3)^{-1}$ also shows a para/ferroelectric behaviour near 300 K ($T_c = 300$ K, $T_0 = 290$ K, $C = 90$ K), which indicates that the incommensurate phase keeps a ferroelectric behaviour. By comparison, for AHSe we (Badot and Colomban 1989) have shown that a small gap occurs between the jump of NH_4^+ and of H^+ relaxation ($\simeq 250$ K) and the jump of the $HSeO_4^-$ relaxation (260 K). The incommensurate phase (250–260 K) of AHSe has thus been related to the presence of both ordered dipole and mobile charges in the structure.

For ADSe the ferro-paraelectric behaviour is clearly observed for the VI⟶II transition ($T_c \simeq 350$ K, $T_0 = 270$ K, $C = 230$ K) for proton relaxation and for the IV⟶II transition ($T_c \simeq 270$ K, $T_0 = 254$ K, $C = 720$ K) for ND_4 relaxation. It can be expected that a sample containing only phase VI will have the lowest value of C.

The situation appears to be rather more complicated for the 250 K phase transition. On cooling, from point {4} we observe a para–ferroelectric transition at about 260 K, with a Curie temperature extrapolated to be $T_0 \simeq 220$ K. Below 260 K, the points {6}, {7}, {8}, $1/\Delta\epsilon$ increases according to the ferroelectric state. However, on heating, a regular increase is observed up to the VI⟶II transition ($T_c = 350$ K). Thus, according to the calorimetric phase diagram, the annealing at 230 K for a week (between points {6} and {7}) has restored the stable sequence, at least as far as the proton ordering is concerned. It can also be concluded that the true T_0 value for the IV⟶III′ transition is in fact lower than 220 K. Between the points {7} and {10}, the behaviour is more complicated. In this way it is necessary to understand the phase stability in the light of theoretical considerations about first-order para–ferroelectric phase transitions.

In the paraelectric phases the temperature dependence of the dielectric stiffness ($1/\Delta\epsilon$) corresponds to the Curie–Weiss expression, $1/\Delta\epsilon = (T - T_0)/C$, where C is the Curie constant. In all cases, since $T_0 < T_c$ (T_c and T_0 are, respectively, the phase transition temperature and the extrapolated Curie temperature), the ferro–paraelectric phase transitions in AHSe and ADSe are of the first-order type. Generally, T_0 represents the limit of metastability of the non-polar paraelectric phase (PE) below a 'first-order' transition temperature. Figure 6(a) schematizes the variation of the dielectric stiffness ($1/\Delta\epsilon$) in relation to the temperature for a hypothetical 'first-order' transition. From the macroscopic theory of Devonshire (Fatuzzo and Merz 1967), which considers the evolution of the free-energy system, it may be possible to define two domains of stability and metastability for the paraelectric and ferroelectric phases (FE). The boundaries of these domains correspond to the temperatures T_0, T_c and T_1, the latter $T_1 (T_1 > T_c)$ representing the limit of metastability of the polar phase (FE) above a 'first-order' transition. We note in the case of a 'second-order' phase transition that $T_0 = T_c = T_1$. Consequently, with the temperature increase different stability and metastability domains can appear.

(i) For $T < T_0$ the ferroelectric phase is stable.

(ii) For $T_0 < T < T_c$ the ferroelectric phase is stable and the paraelectric phase is metastable.

(iii) For $T_c < T < T_1$ the paraelectric phase is stable and the ferroelectric phase is metastable.

(iv) For $T > T_1$ only the paraelectric phase is stable.

From the Glauber model (Lines and Glass 1979) or dynamical Ising model and the Weiss molecular field approximation, T_0 is proportional to J/k. J is defined as the dipole exchange interaction due to the internal molecular field (electric field), which involves only one type of ferroelectric order. This ordering effect can be broken by the thermal motion.

In the case of ND_4^+ relaxation the incommensurate phase III′ corresponds to a paraelectric phase (non-polar phase) where the Curie constant C is higher after annealing than before annealing. The para–ferroelectric phase transition at 270 K is of first order 'near second order', the difference between T_0 (254 K) and T_c (270 K) being small; in this temperature range the paraelectric phase appears metastable before and after annealing (cf figure 6(b)).

In the case of D^+ jump relaxation, the situation is more complicated. In the sequence VI⟶III″ ⟶II the transition temperature $T_c \simeq 350$ K is higher than the extrapolated Curie–Weiss temperature $T_0 = 265$ K. In this temperature range 265–

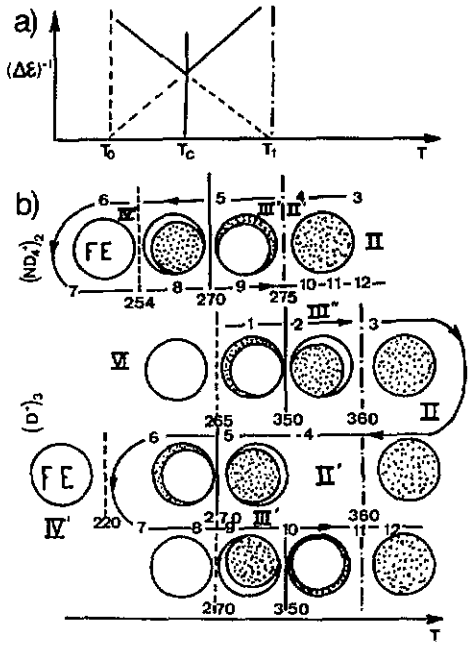

Figure 6. (*a*) Schematization of the variation of the dielectric stiffness $(1/\Delta\epsilon)$ in relation to the temperature for a hypothetical 'first-order' para/ferroelectric phase transition from the macroscopic theory of Devonshire (Fatuzzo and Merz 1967). (*b*) Application of the Devonshire theory to understand the stability and metastability regions in ferroelectic and incommensurate phases of ADSe. Measurement temperatures are located in comparison with the temperatures T_0, T_c and T_1.

350 K the paraelectric phase appears to be metastable. However, in the sequence 3, 4, 5, 6 (II' $\longrightarrow$III' $\longrightarrow$IV'), $T_c = 270$ K, $T_0 = 220$ K and $T_1 \simeq 360$ K (cf figure 6), the metastability region for the ferroelectric phase corresponds to the incommensurate phase III'. The estimated value of T_1 (360 K) corresponds to the end of the peak characterizing the phase transition observed by calorimetric measurements (DSC). Below 220 K (point {7}), the ferroelectric phase only is present and stable. After annealing for a week at 230 K, the heating sequence shows a first-order para–ferroelectric transition at $T_c = 350$ K with $T_0 = 270$ K. Since T_0 goes from 220 K towards 270 K the exchange interaction J between the 'dynamic' dipoles owing to the D^+ jumps has increased. Another type of ferroelectric order thus appears during the annealing at 230 K (the sequence {6 . . . 7}): it probably corresponds to higher J-values, J increasing with time. After a week and during the cycle, J continues to increase towards the value corresponding to kT_0 with $T_0 = 270$ K. It can be expected that a longer duration of the annealing process may restore the initial value (point {1}), as indicated by the arrow of figure 5(*d*). This can be related to the previous observations of well shaped and rather intense DSC peaks at 260 K with crystals annealed a year at 268 K, instead of the typical camel-like feature (two peaks together) of incommensurate phase transitions (Colomban *et al* 1988).

It can be concluded that the ND_4^+ ($\Delta\epsilon_2$) and proton (D) ($\Delta\epsilon_3$) relaxations have different types of behaviours. Two conclusions can be drawn:

(i) in the ferroelectric phase IV', ND_4^+ and the proton contribute to the ferroelec-

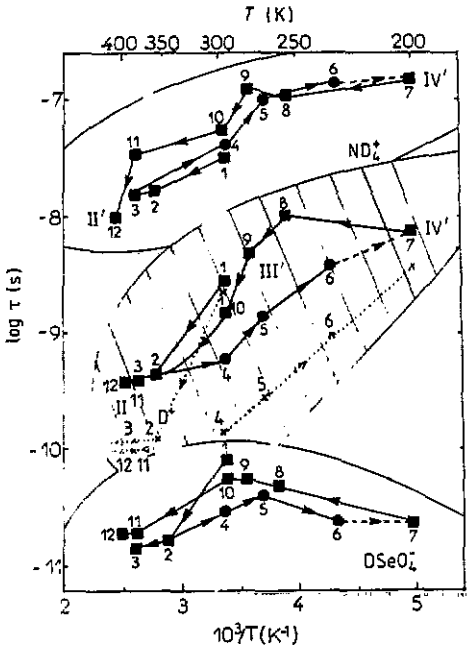

Figure 7. Inverse temperature dependence of dielectric relaxation times τ (full curves) in ADSe corresponding to ND_4^+ and $DSeO_4^-$ reorientations and D^+ jumps. Individual times τ' are given for D^+ relaxation (cross and pointed lines, $\cdots\times\cdots\times\cdots$).

tric state but in the assumed non-ferroelectric phase (VI) a ferroelectric behaviour remains present with ND_4^+ ions;

(ii) the disappearance of the ferroelectric order induced by annealing at low temperature to develop the stable sequence is more rapid for protons than for ammonium ions.

The time needed to restore the stable sequence seems to be related to diffusion phenomena which need time. Such diffusion-controlled transitions are observed in all acid sulphates (selenates).

The plot of the inverse susceptibility of ND_4^+ relaxation exhibits for both {4}, {5}, {6}, {7} and {7}, {8}, {9}, {10} sequences of measurement, a para–ferroelectric behaviour. As discussed for the 350 K transitions with proton susceptibility ($1/\Delta\epsilon_3$), the value of T_0 remains constant but the value of C goes from 350 K before annealing (phase IV') to 720 K after annealing (⟶phase VI), if the product $N\mu^2$ decreases. We have the same type of behaviour for ND_4^+ and proton relaxation. With the lack of other measures between 230 and 270 K it is difficult to be precise if ND_4^+ and D^+ relaxations exhibit a change $1/\Delta\epsilon$ at the same temperature.

3.5. Relaxation times

Figure 7 shows a logarithmic law for the different relaxations: τ_4 ($DSeO_4^-$), τ_3 (D^+) and τ_2 (ND_4^+). The mean value is consistent with previous correlations (Colomban and Novak 1988, Colomban and Badot 1992). The conclusions discussed with $1/\Delta\epsilon = f(T)$ plots (figure 5) can be confirmed in figure 7. Some new information can, however, be observed. The room temperature τ_4 values (cf table 1) are slower than in $CsDSeO_4$ (8.4×10^{-12} s) and AHSe (9.7×10^{-12} s) (Badot and Colomban 1989). The

main characteristic is the 'hysteresis' observed with τ_3 between cooling (metastable sequence II′ $\longrightarrow$IV′) and heating (stable VI$\longrightarrow$II sequence). The discrepancy is larger than the error of the measure. This 'hysteresis' gives a picture of the local changes induced by the ferroelectric ordering. The larger change is thus observed for D^+ motions. A plot of the individual times τ' according to the molecular-field approximation (Makita and Seo 1969) ($\tau' = C\tau/T\Delta\epsilon$) increases the hysteresis, which can be considered as an effect arising from a local configuration and from the crystal-field changes in the framework.

4. Conclusions

A microscopic analysis of the transitions occurring in both structures with fixed charges (involving ferroelectric/paraelectric behaviour) and with mobile charges (ionic conductor) has shown that different kinds of sublattice contribute to the macroscopic electric behaviour (an analogy can be made with magnetic ordering on different sublattices) and that its contribution can increase (decrease) with temperature with different laws. It is thus possible to have simultaneously mobile (proton) and fixed charges in the structure. A dynamical view of the charges is needed to get a better understanding of the phase transition mechanisms. In the acid selenate (sulphate) family, the most important dipoles arise from the translation-fixed distorted ammonium tetrahedron except in the superionic phase where proton jump relaxation is predominant. Below the superionic phase transition the selenate ion reorientation stiffness increases. The existence of the incommensurate phase seems to be related to the different rates in the evolution of ordered sublattices. Memory effects at the local scale are in evidence and this behaviour seems to be related to the time needed to restore a stable configuration by diffusion of the protons.

Acknowledgment

Professor A Fourrier-Lamer is acknowledged for allowing us the use of her laboratory facilities.

References

Aleksandrov K S, Kruglik A I, Misyul S V and Simonov M A 1980 *Sov. Phys.–Crystallogr.* **25** 654

Aleksandrova I P, Colomban Ph, Dénoyer F, Le Calvé N, Novak A, Pasquier B and Rosycki A 1989 *Phys. Status Solidi* a **114** 531

Aleksandrova I P, Moskvich Yu N, Rozanov O V, Sadreev A F, Seryvkova I V and Sukhovskii A A 1986 *Ferroelectrics* **67** 63

Aleksandrova I P, Rozanov O V, Sukhovski A A and Moskvich Yu N 1983 *Phys. Lett.* A **15** 339

Badot J C, Baffier N and Fourrier-Lamer A 1985 *J. Physique* **46** 2107

Badot J C and Colomban Ph 1989 *Solid State Ionics* **35** 143

Badot J C, Fourrier-Lamer A, Baffier N and Colomban Ph 1987 *J. Physique* **48** 1327

Badot J C, Fourrier-Lamer A, Mhiri T and Colomban Ph 1991 *Solid State Ionics* **46** 151

Baranov A T, Shuvalov L A and Shagina N M 1982 *JETP Lett.* **36** 459

Colomban Ph and Badot J C 1992 *Proton Conductors* ed Ph Colomban (Cambridge: Cambridge University Press)

Colomban Ph and Novak A 1988 *J. Mol. Struct.* **177** 277

Colomban Ph, Rosycki A and Novak A 1988 *Solid State Commun.* **67** 969

Czapla C, Czupinski O and Sobczyk L 1984 *Solid State Commun.* **51** 309
Czapla C, Lis T and Sobczyk L 1979 *Phys. Status Solidi* a **51** 609
Debye P 1945 *Polar Molecules* (New York: Dover)
Dygas J R and Brodwin M E 1985 *Solid State Ionics* **18–19** 981
Fatuzzo E and Merz W J 1967 *Ferroelectricity* (Amsterdam: North-Holland)
Hainovsky N G and Hairetdinov E F 1985 *Izv. Sib. Otd. Akad, Nauk. SSSR Ser. Khim. Nauk.* **8** 33 (in Russian)
Jonsher A K 1983 *Dielectric Relaxation in Solids* (London: Chelsea Dielectric Press)
Lines M E and Glass A M 1979 *Principles and Applications of Ferroelectrics and Related Materials* (Oxford: Clarendon)
Makita Y and Seo I 1969 *J. Chem. Phys.* **51** 3058
Moskvich V N, Sukhovsky A A and Rozanov O V 1984 *Fiz. Tverd. Tela* **26** 38 (Engl. Transl. 1984 *Sov. Phys.–Solid State* **26** 21)
Pasquier B, Le Calvé N, Rozycki A and Novak A 1990 *J. Raman Spectrosc.* **21** 465
Richards P M 1977 *Phys. Rev.* B **16** 1393
Volkov A A, Kozlov G V and Petzelt J 1989 *Ferroelectrics* **95** 23